Electronic Supplementary Information

Supramolecular Engineering of Cathode Materials for Aqueous Zinc-ion Hybrid Supercapacitors: Novel Thiophene-bridged Donor-Acceptor sp^2 Carbon-linked Polymers

Haijun Peng,[a] Verónica Montes-García,[a] Jésus Raya,[b] Hanlin Wang,[a] Haipeng Guo,[a] Fanny Richard,[a] Paolo Samorì *[a] and Artur Ciesielski*[a]

[a] Université de Strasbourg, CNRS, ISIS 8 allée Gaspard Monge, 67000 Strasbourg, France

[b]Université de Strasbourg, CNRS, Membrane Biophysics and NMR, Institute of Chemistry, 1 Rue Blaise Pascal, 67000 Strasbourg, France

E-mail: samori@unistra.fr, ciesielski@unistra.fr

Table of Contents

Section A. Materials and characterization

Materials

All commercially available reagents and solvents were purchased from Sigma Aldrich and used as received without further purification**.** Zinc foil (thickness of 100 µm), Stainless steel gauze and coin cells cases were obtained from Alfa Aesar and S4R France, respectively. The nonwoven fabric membrane (NKK-MPF30AC-100) was purchased from Nippon Kodoshi Corporation (kochi, Japan). 2, 5-Thiophene dicarboxaldehyde (TDA) and [2,2'-Bithiophene]-5,5'-dicarboxaldehyde (BTDA) were purchased from TCI. **2**,2',2''-(benzene-1,3,5-triyl)triacetonitrile (BTAN) was prepared according to the previous reported procedure.[1]

Characterization

The composition, structure, and texture properties of materials were investigated by X-ray powder diffraction (XRD) patterns (Bruker D8 X-ray diffractometer), Fourier transform infrared (FT-IR) spectra were recorded using a FT-IR 4700 Fourier Transform Infrared Spectrometer (JASCO) equipped with ATR Diamond. Thermogravimetric analyses (TGA) decomposition curves were recorded in the range 25-800 °C operating under nitrogen *atmosphere*, with a thermal step of 10 °C/min on a Mettler Toledo TGA/SDTA851e system. The specific surface area was measured using a Micromeritics ASAP 2050 surface area and porosity analyzer. Before the BET measurements, the samples were outgassed for 10 hours at 100 °C. Adsorption isotherms were calculated for nitrogen adsorption at 77 K and pressure up to 1 bar. Scanning Electron Microscopy (SEM) images and Energy-dispersive X-ray spectroscopy (EDX) were recorded with a FEI Quanta FEG 250 instrument S3 (FEI corporate, Hillsboro, Oregon, USA). X-ray Photoelectron Spectroscopy (XPS) (Thermo Scientific K-Alpha X-ray photoelectron spectrometer) equipped with an aluminum X-ray source (energy 1.4866 keV) at a vacuum level of 10^{-8}-10^{-9} mbar in the main chamber. The spot size of the X-ray beam was fixed at 400 µm. The ultraviolet photoelectron spectroscopy (UPS) was measured via He I (21.2eV) as excitation sources at a base pressure at 10^{-10} Torr in Thermo VG Microtech VSW 5000. Scanning transmission electron microscopy (STEM) was performed on a FEI Quanta FEG 250 instrument S3 (FEI corporate, Hillsboro, Oregon, USA). The samples were prepared by depositing 7 µL of a dispersion on a TEM grid covered by a lacey carbon membrane. The as-prepared grids were kept overnight under a high vacuum to remove the eventual solvent residues and possible contaminants.

Solid-state MAS NMR experiments were performed at room temperature on an AVANCE 750 MHz wide bore spectrometer (Bruker™) operating at a frequency of 750.12 MHz for ^{1}H and 188.5 MHz for ^{13}C. ^{1}H spectra were obtained by spinning all samples at 59.523 kHz in a triple resonance $^{1}H/^{13}C/^{15}N$ Ultra-Fast MAS probe (Bruker™) designed for 1.3 mm o.d. zirconia rotors while ^{13}C spectra were recorded in a double resonance MAS probe (Bruker™) allowing samples to be spun at 29.762 kHz after packing them inside 2.5 mm o.d. zirconia rotors (each type of rotors closed with vessel caps). In order to get undistorted line shapes and filter out background probes signals a speed synchronized spin echo [1] was included inside the experimental pulse sequences for both nuclei. We should mention here that this kind of spin-echo (P_{90}-τ-P_{180}- τ) is possible for protons only because we are spinning fast enough to highly reduce the homonuclear dipolar interactions. Raw data were processed with a 20 Hz Lorentzian filter followed by Fourier transformation without zero filling.

Preparation of three electrode system

The preparation of the three-electrode system for the calculation of the HOMO and LUMO levels was as follows: donor-acceptor carbon-conjugated polymer (DA-CCP)-1or -2 samples were dispersed in ethanol with a few droplets of 5 wt% Nafion and grind in agate mortar for half an hour, then the obtained suspension was drop casted on a glassy carbon electrode and air-dried to form thin films for measurements. The cyclic voltammetry (CV) experiments were executed with an Autolab PGSTAT 128N instrument in a three-electrode electrochemical cell with a scan rate of 0.02 V s^{-1}. The experiments were conducted in anhydrous acetonitrile with tetrabutylammonium hexafluorophosphate (0.1M) as supporting electrolyte. The auxiliary electrode was a platinum plate, and Ag/AgCl was used as reference electrode.

The ferrocene/ferrocenium (F_c/F_c^{+}) redox potential was measured at the end of each experiment in order to calibrate the pseudo reference electrode as recommended by IUPAC.

The HOMO and LUMO levels were determined using the following formulas:

EHOMO=-[Eox-E(FC/FC^{+}) +4.8] eV

ELUMO=-[Ered-E(FC/FC^{+}) +4.8] eV

Fabrication of Zn-HSCs

Zinc foil was directly used as an anode electrode after being polished with gauze and pouched into electrodes with 12 mm diameter. The cathode electrode was composed by a mixture of 70 wt% of DA-CCP-1 or -2, 20 wt% of multi-walled carbon nanotubes (MWCNT), and 10 wt% of polytetrafluoroethylene (PTFE) as the binder. Ethanol solvent was added to the above mixture and then the mixture was coated onto stainless steel gauze. The electrodes were dried in a vacuum oven at 80℃ overnight. Zinc-ion hybrid supercapacitors were assembled with the electrolyte of 2 M $Zn(CF_3SO_3)_2$ aqueous solution, nonwoven fabric membrane (NKK-MPF30AC-100) as separator, and coin-shaped cell. The mass loading of the active material is 1.7~ 2.2 mg cm^{-2}.

Electrochemical characterization and calculations of Zn-HSC

The electrochemical performance of Zn-HSC was studied using cyclic voltammetry (CV) and electrochemical impedance spectroscopy (EIS) on Autolab PGSTAT128N Potentiostat / Galvanostat instruments with a Metrohm Autolab DuoCoin Cell Holder (Metrohm AG) at room temperature. CV was performed at scan rates of 0.1 - 100 mV s-1 in the voltage range between 0 and 1.6 V. EIS was recorded from 0.01 Hz to 1 MHz, swept from high to low frequencies, with a sine-wave voltage signal amplitude of 50 mV (root-mean-square, RMS). The galvanostatic charge-discharge (GCD) tests were carried out on Neware Battery Tester (BTS-4008T-5V/10mA, Neware Technology Company, Guangdong, China). GCD curves were tested at current densities ranging from 0.1 to 5 A g-1.

The capacity is obtained from the software (Neware BTS 7.6), and the coulombic efficiency was obtained by the division of: charging capacity /previous discharging capacity ∗100%.The energy density, E, and power density, P, were calculated following these equations:

$$E = \int V \times I dt/m \tag{1}$$

$$P = \frac{E}{t} \tag{2}$$

where V is average discharge voltage, m is DA-CCP -1 or -2 electrode mass, I is the discharging current, t is the time hour. The accurate value is obtained from the integral computation given by the analysing software (Neware BTS 7.6)of the testing instrument. The sheet resistance of DA-CCP-1 and -2 was measured using a four-point probe (Jandel, Model RM3000) on a pressed pellet with a thickness of ~100 um, The bulk conductivity was calculated by using following the equations:

$$\sigma = \frac{1}{t \cdot Rs} \tag{3}$$

where σ is conductivity, t is thickness and Rs is sheet resistance.

Synthesis of 2,2',2''-(benzene-1,3,5-triyl)triacetonitrile (BTAN): Prepared as previously reported.[1] To a solution of 1,3,5-tris(bromomethyl)benzene (3.02 g, 8.50 mmol) in THF (25 mL), sodium bicarbonate (saturated solution, 30 mL) and sodium cyanide (4.17 g, 85.0 mmol) were added followed by 30 mL water. The solution was left under stirring for 3 days after which it is was acidified with 1 M HCl. Tetrahydrofuran (THF) was removed via rotary evaporation to obtain 1.46 g (88%) of an off-white solid. ^{1}H NMR ($CDCl_3$, δ (ppm)): 7.31 (s, 3 H), 3.80 (s, 6 H), IR: ν 2239 cm^{-1} (C≡N).

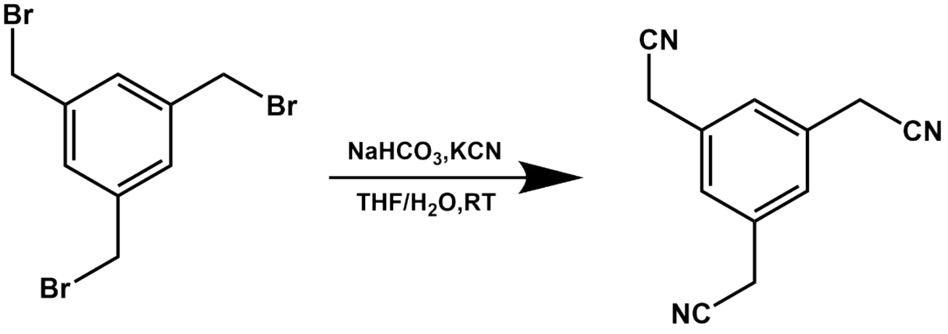

Fig. S1. Synthesis route for BTAN.

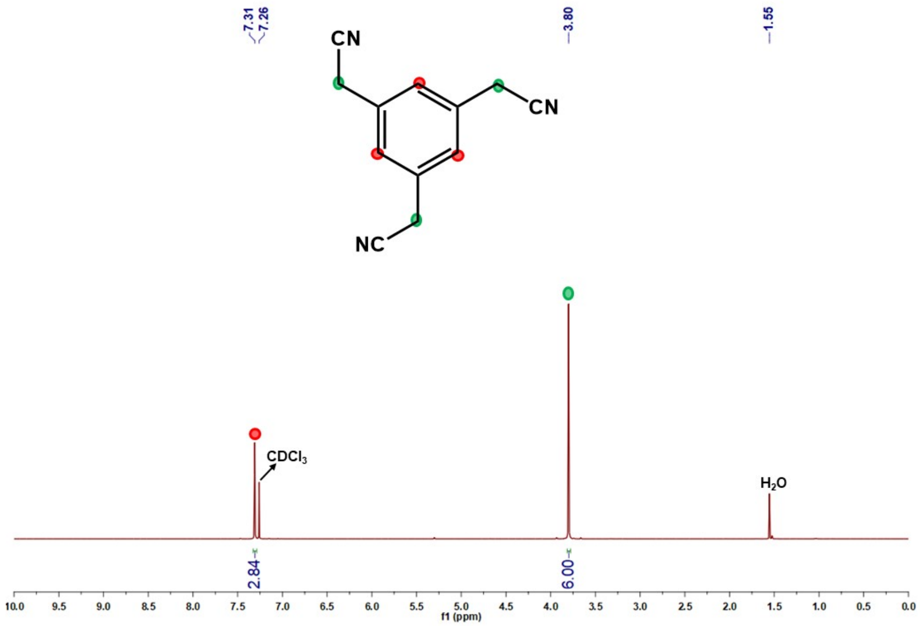

Fig.S2. ^{1}H NMR spectra (400 MHz, $CDCl_3$) of BTCN: δ 3.80 (s,6H), 7.31 (s,3H) ppm.

Synthesis of model compound: In a typical experiment, 2-thiophenecarboxaldehyde (5 mmol) was added to BTAN (5.7 mmol) in 70 ml of ethanol, followed by the addition of 0.35 mmol of potassium tert-butoxide (t-BuOK). A yellow precipitate was formed immediately, and the solution was kept under stirring for another hour. Finally, the precipitate was filtered, washed with ethanol and was dried leading to a yellow solid (yield 80%). ^{1}H NMR ($CDCl_3$, δ(ppm)): 7.20 (s, 3 H), 7.63 (s, 3H), 7.76 (s, 3 H), 7.81 (s, 3 H), 7.83 (s, 3 H).

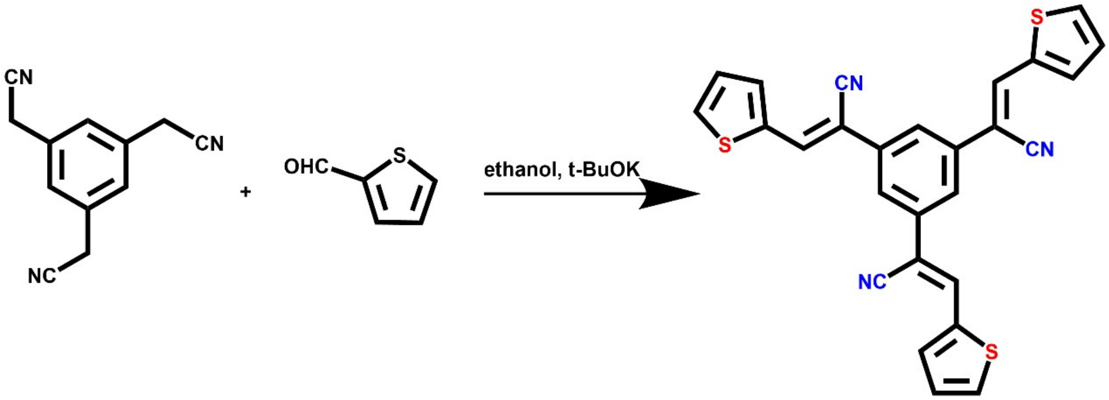

Fig. S3. Synthesis route for the model compound.

Synthesis of DA-CCP-1 and -2. The synthesis conditions for DA-CCP-1 synthesis are: a mixture of 2,2',2''-(benzene-1,3,5-triyl)triacetonitrile (BTTA 28.1 mg, 0.144 mmol), 2, 5-Thiophene Dicarboxaldehyde (TDA 29.5 mg, 0.21 mmol), dimethylacetamide (DMA, 2 mL) and o-dichlorobenzene (o-DCB, 2 mL) was placed in a 10 mL micro-reaction vessel. The vessel was charged with nitrogen by flowing nitrogen gas for 3 min, then caesium carbonate (Cs_2CO_3 68.4 mg, 0.21 mmol) which dissolved in 200 µl H_2O was added and nitrogen gas was flowed again for 3 min. Then the vessel was sealed by screwing the cover tightly and heated at 120 °C for 3 days. The conditions for DA-CCP-2 synthesis were the same as DA-CCP-1,except for using [2,2'-Bithiophene]-5,5'-dicarboxaldehyde (BTDA 46.8 mg, 0.21 mmol) instead of TDA. The resulting precipitates were collected by centrifugation, subjected to Soxhlet extraction with anhydrous orthodichlorobenzene methanol, and tetrahydrofuran for 24 h for each solvent, and then were dried to produce the DA-CCP-1 and -2 in 85% and 89% isolated yields, respectively.

Section B. Physical Characterization

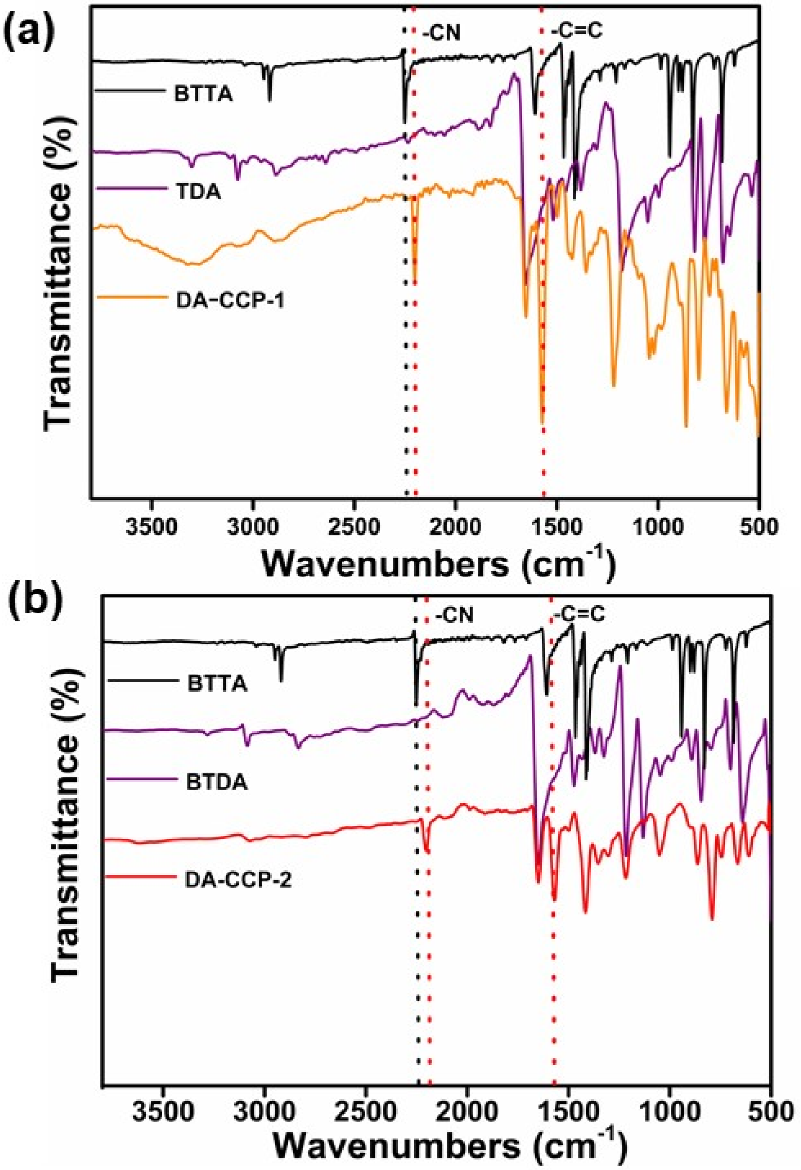

Fig. S4. FT-IR spectra of (a) DA-CCP-1 and (b) DA-CCP-2 compared with their respective monomers.

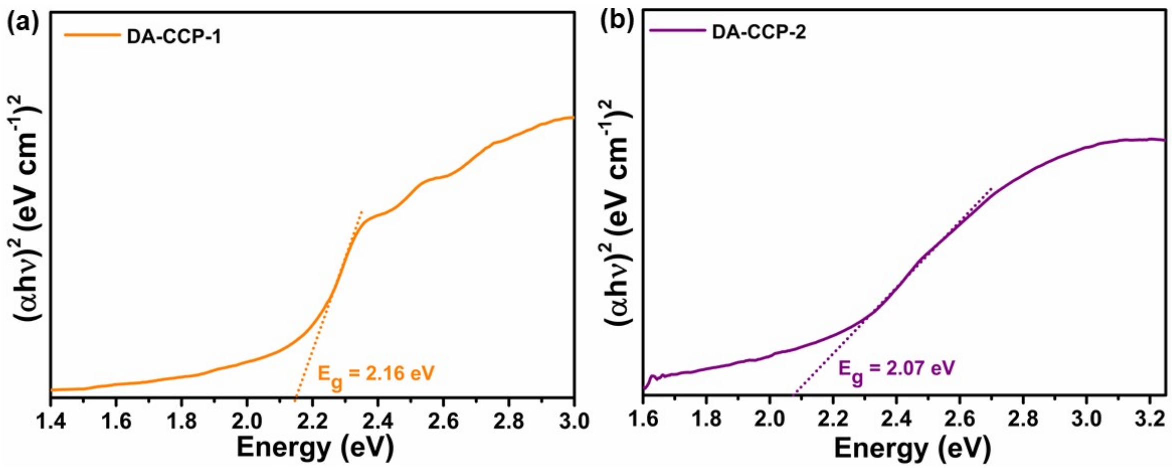

Fig. S5. Tauc plot analysis of UV-vis absorption spectrum of (a) DA-CCP-1 and (b)DA-CCP-2.

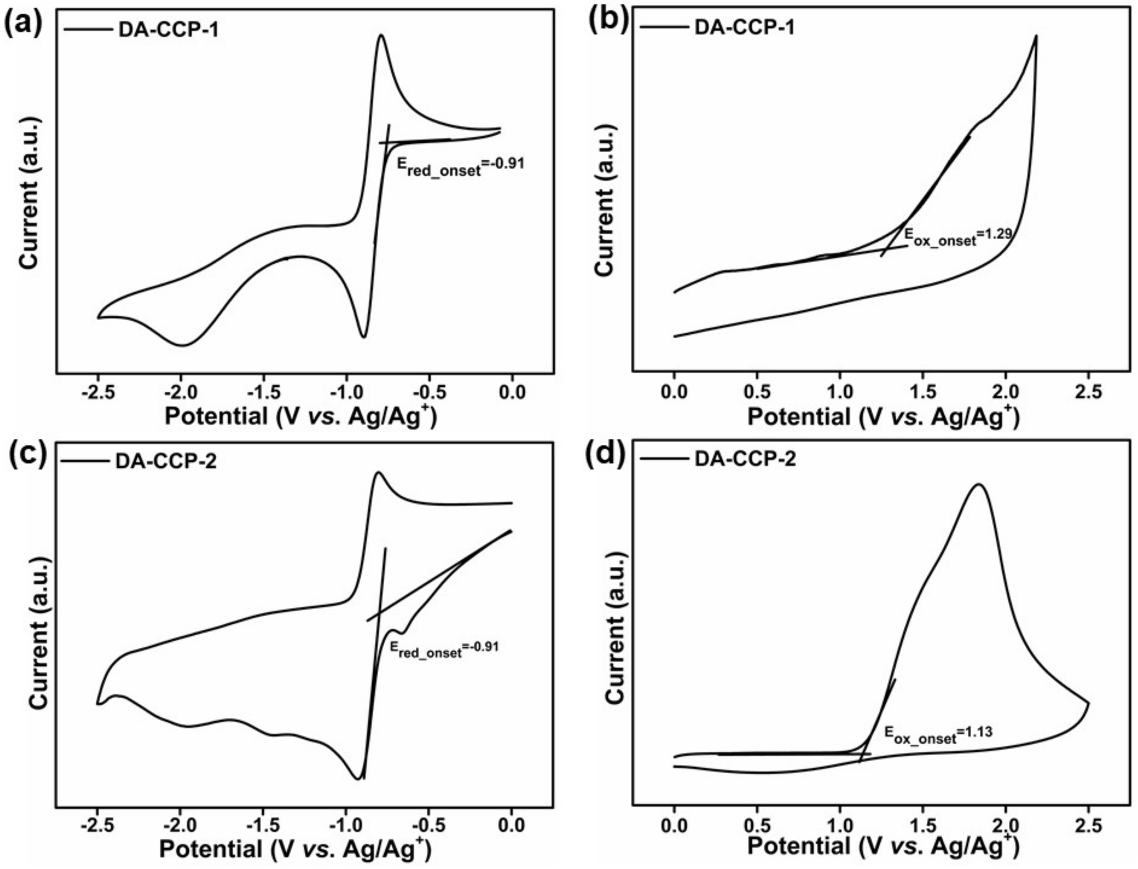

Fig. S6. CV of DA-CCP-1 and -2 at scan rates of 10 mV s^{-1}.

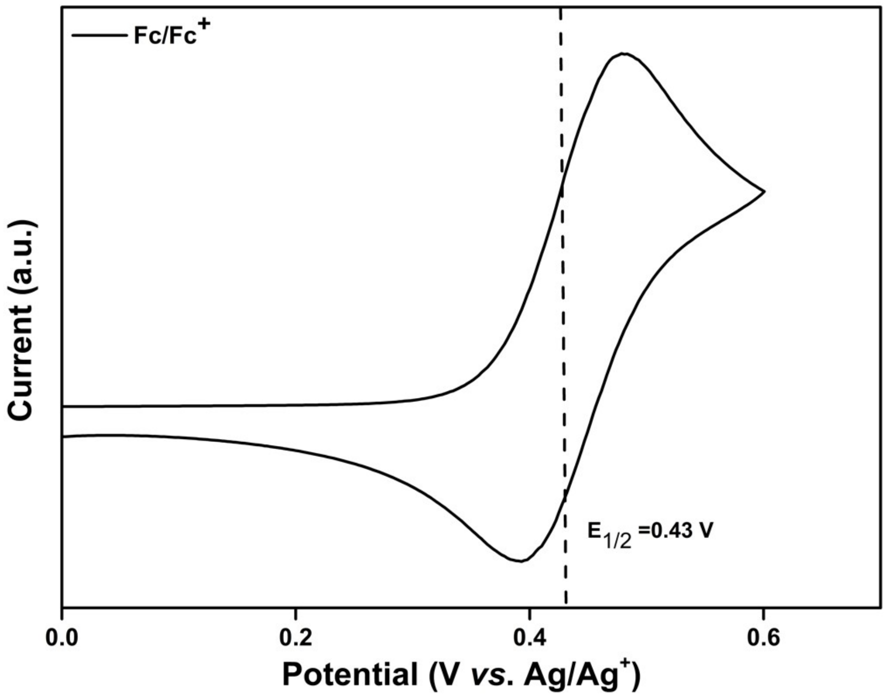

Fig. S7. CV of ferrocene/ferrocenium.

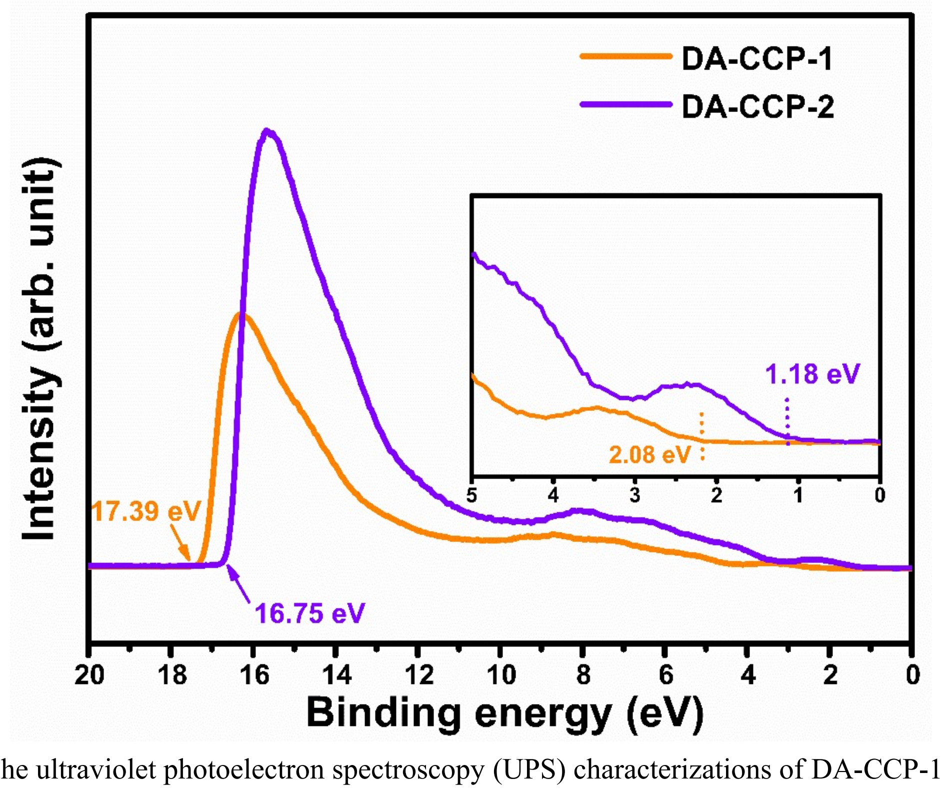

Fig. S8. The ultraviolet photoelectron spectroscopy (UPS) characterizations of DA-CCP-1 and -2.

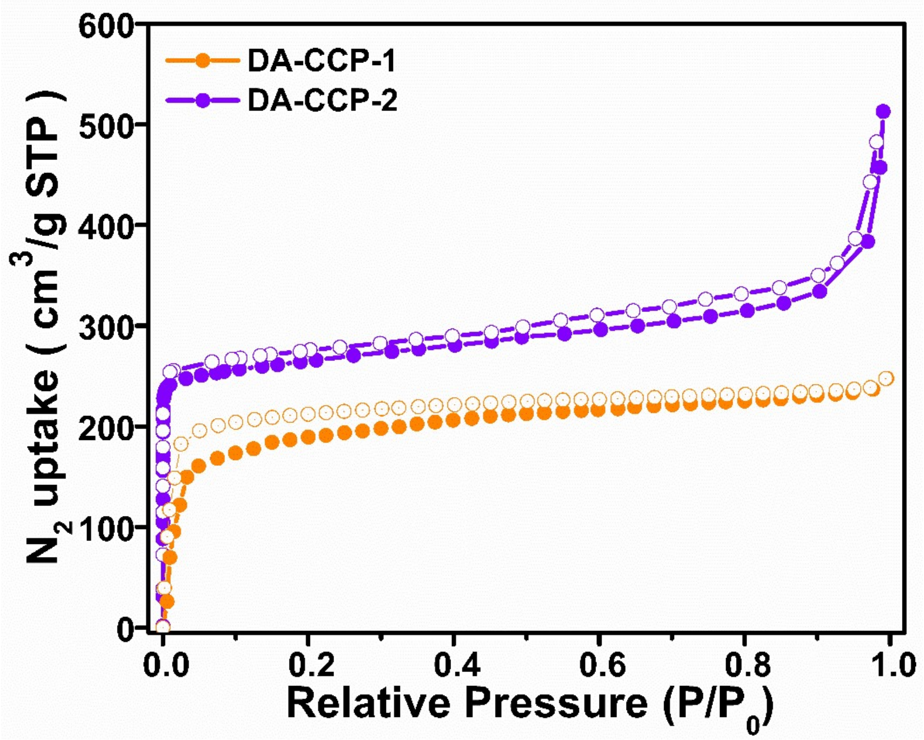

Fig. S9. BET surface area of DA-CCP-1 and -2 (orange and purple curves respectively).

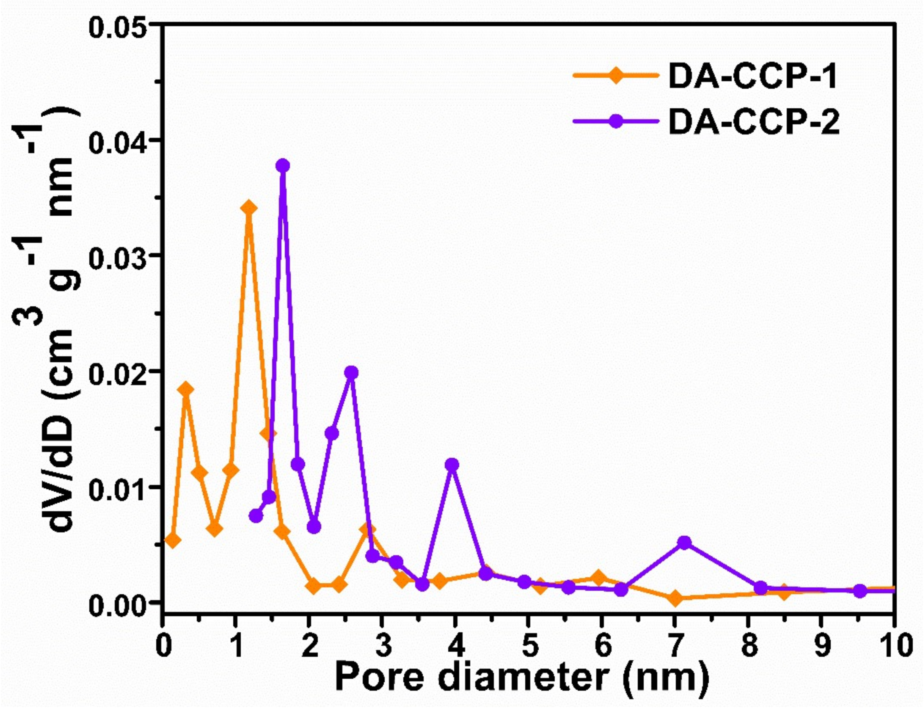

Fig. S10. Pore size distribution of DA-CCP-1 and -2 (orange and purple curves respectively).

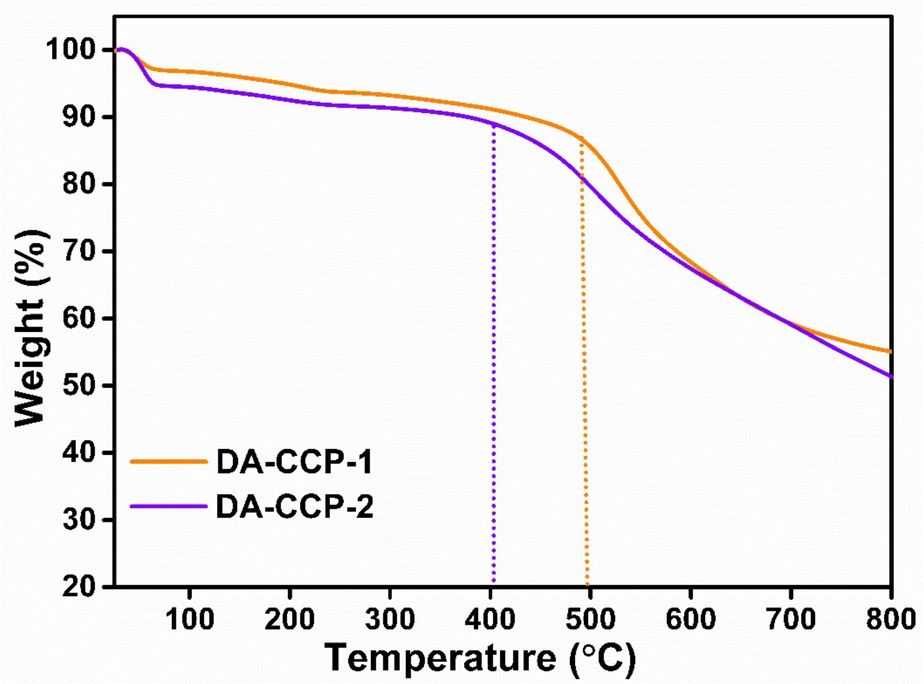

Fig. S11. Thermogravimetric analysis (TGA) curves of DA-CCP-1 and -2 (orange and purple curves respectively).

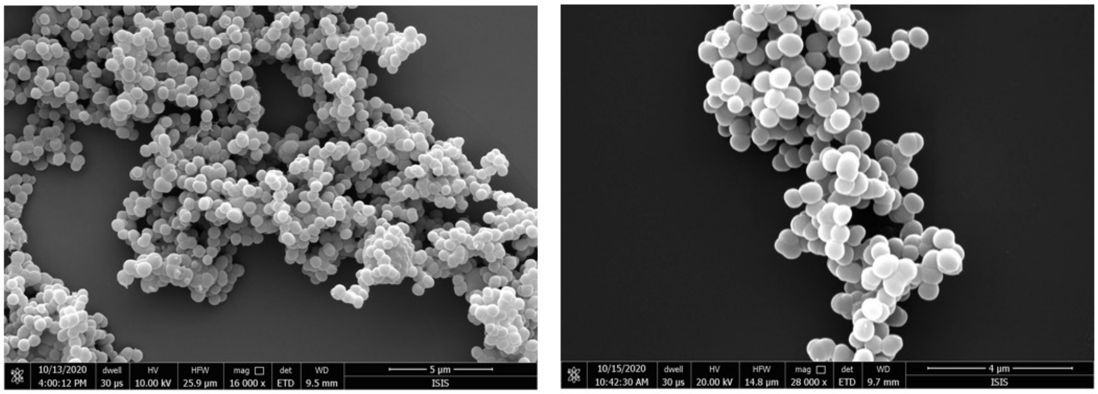

Fig.S12. SEM images of DA-CCP-1.

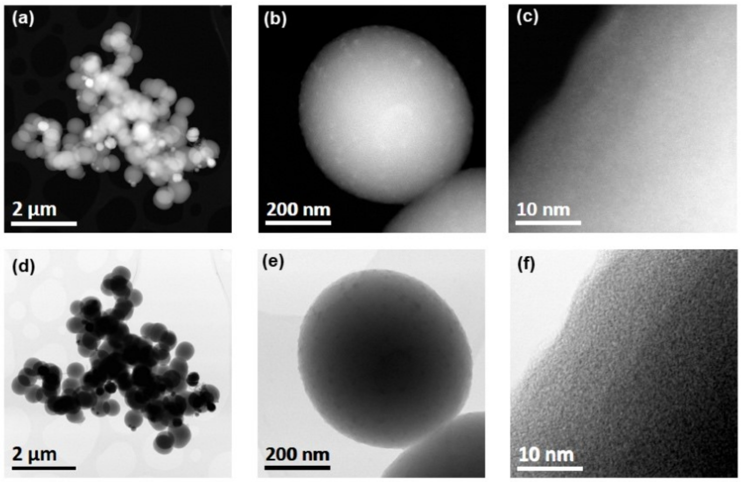

Fig. S13. STEM images of DA-CCP-1 in (a, b, c) dark and (d, e, f) bright fields.

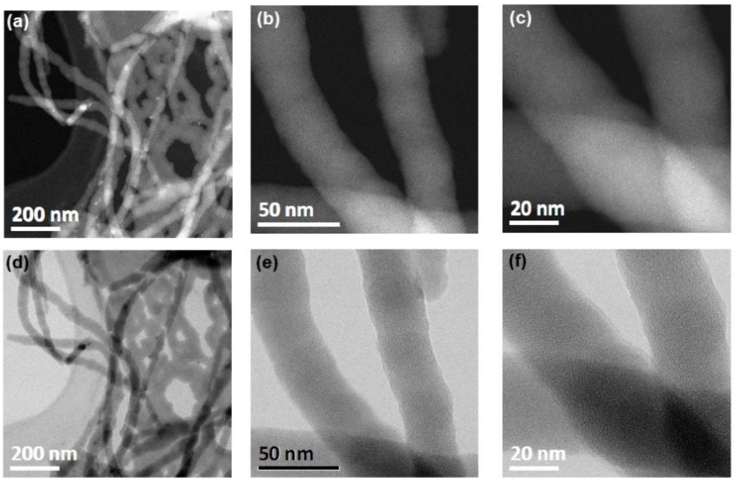

Fig. S14. STEM images of DA-CCP-2 in (a, b, c) dark and (d, e, f) bright fields.

Section C. Electrochemical Measurements

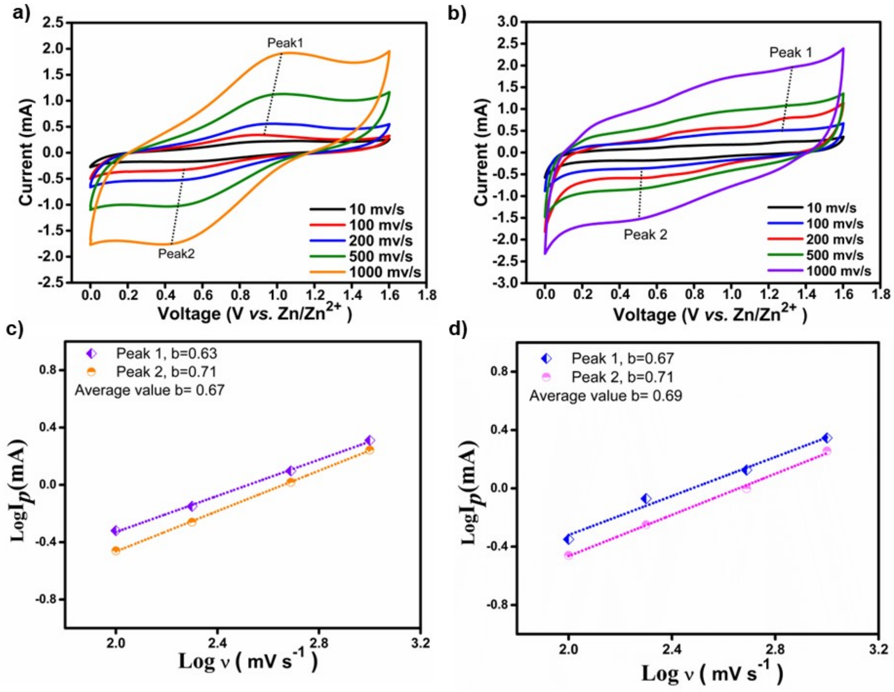

Fig. S15. Electrochemical kinetics study of DA-CCP-1 and -2. a-b) CV curves at various scan rates for a) DA-CCP-1 and b) DA-CCP-2, c-d) The linear fits of I log vs log ν plots to calculate b values according to the equation of $i=a\nu^b$ for c) DA-CCP-1 and d) DA-CCP-2.

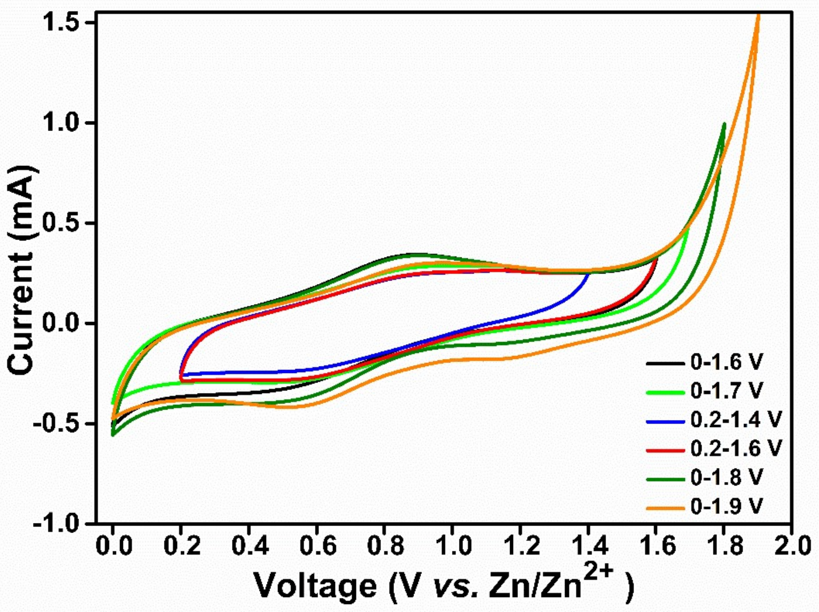

Fig. S16. CV of DA-CCP-1 at different potential windows.

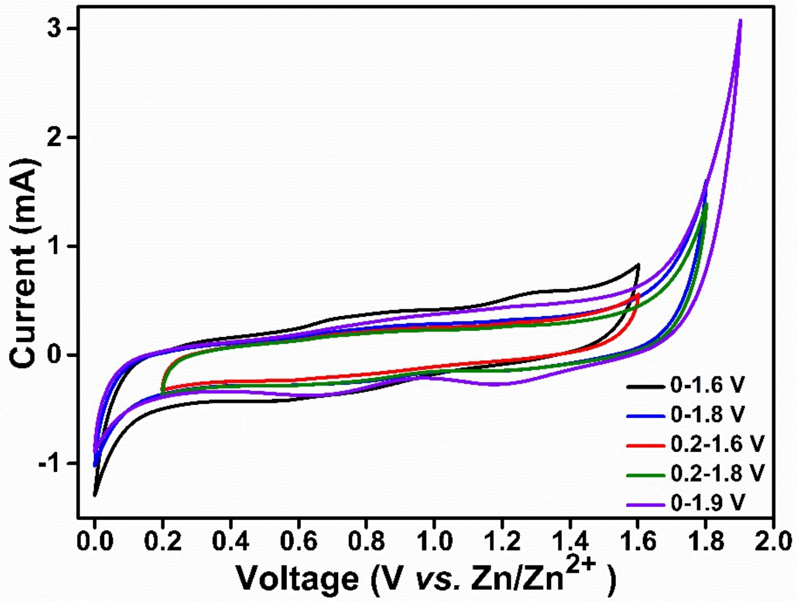

Fig. S17. CV of DA-CCP-2 at the different potential windows.

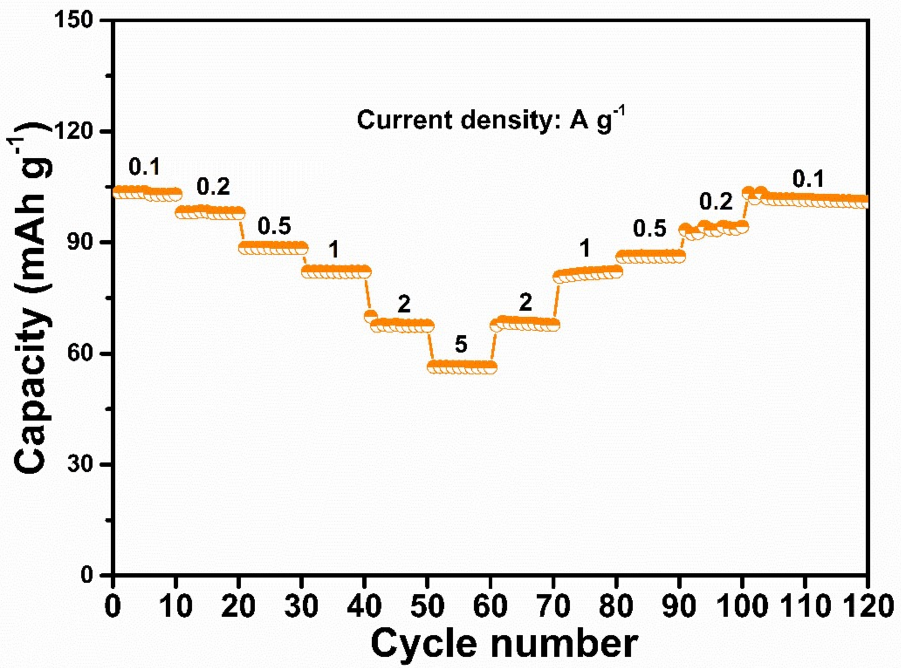

Fig. S18. The rate performance of DA-CCP-1 cathode in Zn-HSCs.

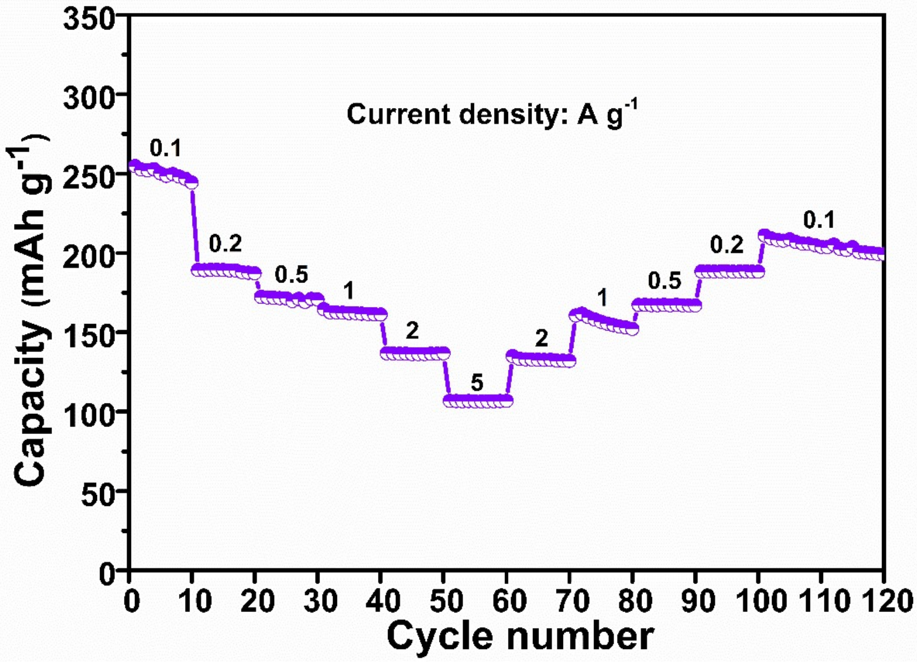

Fig. S19. The rate performance of DA-CCP-2 cathode in Zn-HSCs.

Table S1. Gravimetric capacity of our DA-CCP-1 and DA-CCP-2 electrodes compared to recently reported COFs and other reported cathode materials for aqueous Zn^{2+} energy storage.

Material type	**Electrode**	**Electrolyte**	**Voltage (V)**	**Current density / A g^{-1}**	**Capacity / mA g^{-1}**	**Ref**
Inorganic compounds	ZMO/C	3M $Zn(CF_3SO_3)_2$	0.8-1.9	0.5	150	2
				0.2	72	
	$H_2V_3O_8$ nanowire	3M $Zn(CF_3SO_3)_2$	0.2-1.6	0.5	279	3
				5	155	
	HfO_2-coated ZVO	1M $ZnSO_4$	0.2-1.8	0.1	215	4
				3	88	
	Mesoporous carbon spheres	2M $ZnSO_4$	0.2-1.8	0.1	174.7	5
				5	108.7	
	ZMO@Ti3C2 Tx	1M $ZnSO_4$ 0.05M $MnSO_4$	0.8-1.8	0.2	150	6
				4	84.5	
Organic compounds	C4Q	3M $Zn(CF_3SO_3)_2$	0.2-1.8	0.25	220	7
				1	172	
	Tetrachloro-1,4 benzoquinone	1 M $Zn(CF_3SO_3)_2$	0.8-1.4	0.217	118	8
	PQ-D	3M $Zn(CF_3SO_3)_2$	0.25-1.6	0.03	225	9
				0.15	210	
	DTT	2M $ZnSO_4$	0.3-1.4	0.2	175	10
				2	99	
	Phenothiazine	2M $ZnSO_4$	0.5-1.7	0.04	188.24	11
				0.1	145.56	
COFs	PI-COF	2M $ZnSO_4$	0.9-0	0.7	92	12
	PA-COF	1M ZnSO4	0.2-1.6	0.1	247	13
				5	93	
	HqTp	3M $ZnSO_4$	0.2-1.8	0.125	276	14
				3.75	85	
	HA-COF	2M $ZnSO_4$	0.2-1.6	0.1	339	15
				5	170	
	Tp-PTO-COF	2M $ZnSO_4$	0.4-1.5	0.2	301.4	16
				5	192.8	
Polymer	PDA	3.3 M $ZnSO_4$	0.3-1.4	0.2	85	17
				5	43.2	
	CLPy	30 M $ZnCl_2$	0.5-1.8	0.2	150	18
				3	105	
	DA-CCP-1	**2M $Zn(CF_3SO_3)_2$**	**0.2-1.6**	**0.1**	**103.4**	**This work**
				5	**57.8**	
	DA-CCP-2	**2M $Zn(CF_3SO_3)_2$**	**0.2-1.6**	**0.1**	**251.7**	
				5	**101.2**	

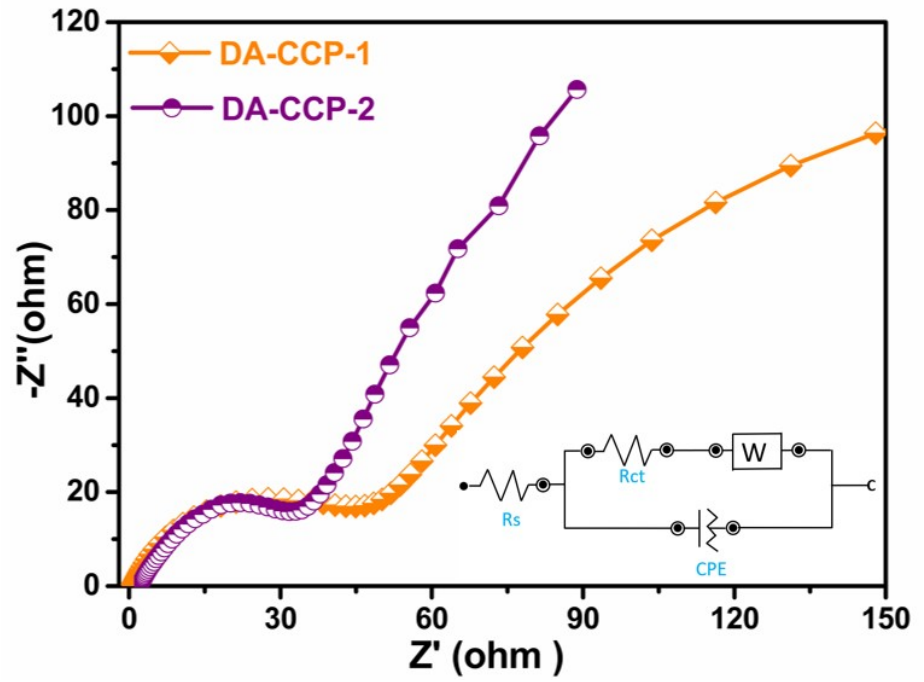

Fig. S20. Electrochemical impedance spectroscopy (EIS) analysis of DA-CCP-1 and -2 cathodes (orange and purple curves respectively). R_s: the intrinsic ohmic resistance; R_{ct}: charge transfer resistance; CPE: constant phase element representing the electrical double layer capacitance (EDLC); W: a generalized finite Warburg element.

Table S2. Circuit parameters for the EIS measurements of DA-CCP-1.

Element	**Parameter**	**Value**	**Estimated Error (%)**
Rs	R	0.637 Ω	1.825
Rct	R	23.839 Ω	1.140
CPE	Y0	0.025823	6.802
C	C	2.5706 µF	1.083
	N	0.68342	0.964
Z_W	Y0	0.46192	2.252
	χ^2	0.078317	

Table S3. Circuit parameters for the EIS measurements of DA-CCP-2.

Element	**Parameter**	**Value**	**Estimated Error (%)**
Rs	R	1.632 Ω	1.736
Rct	R	17.832 Ω	1.140
CPE	Y0	0.042583	5.802
C	C	5.8703 µF	1.180
	N	0.88347	0.729
Z_W	Y0	0.58749	2.745
	χ^2	0.065214	

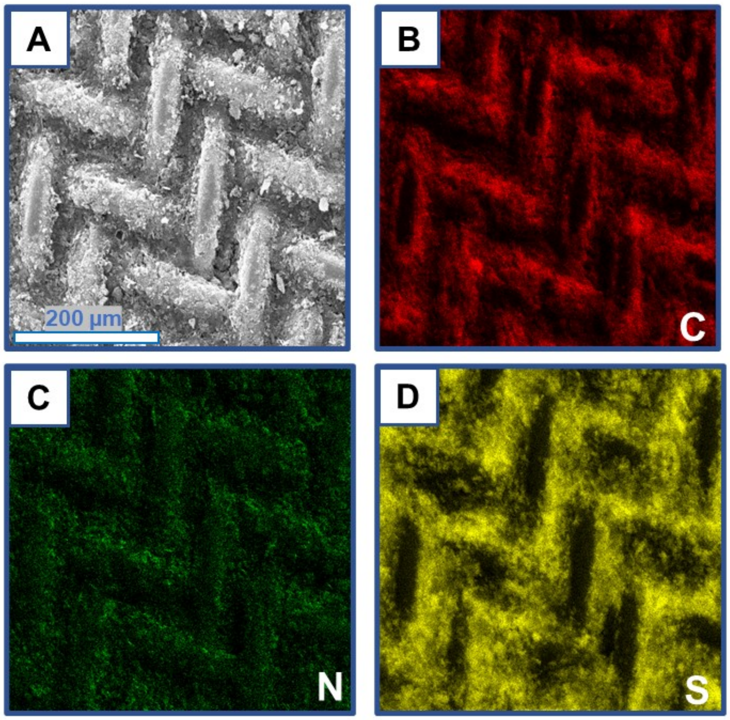

Fig. S21. EDS analysis results of DA-CCP-1 pristine electrode. (a) SEM image, (b) EDS map of C, (c) EDS map of N, (d) EDS map of S.

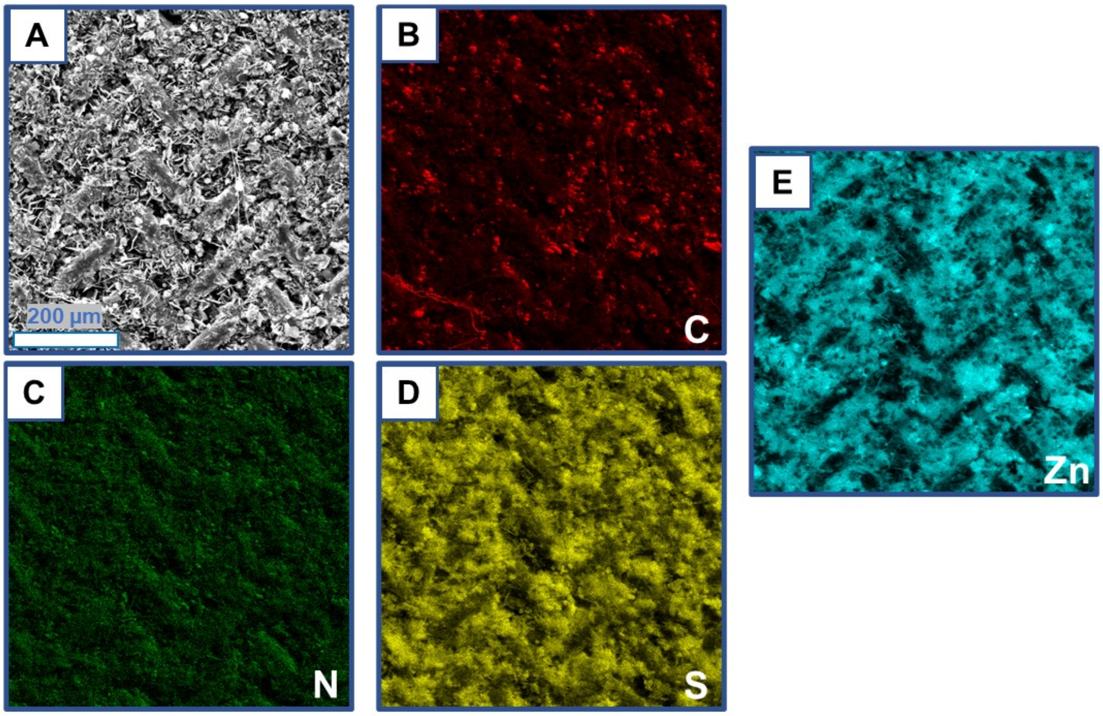

Fig. S22. EDS analysis results of DA-CCP-1 electrode after 1000 cycles. (a) SEM image, (b) EDS map of C, (c) EDS map of N, (d) EDS map of S, (e) EDS map of Zn.

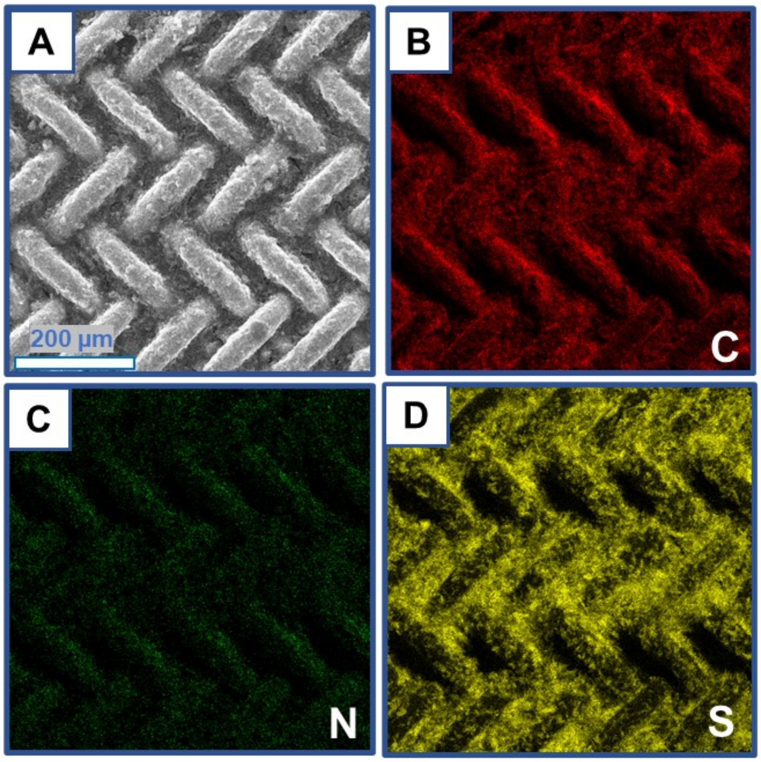

Fig. S23. EDS analysis results of DA-CCP-2 pristine electrode. (a) SEM image, (b) EDS map of C, (c) EDS map of N, (d) EDS map of S.

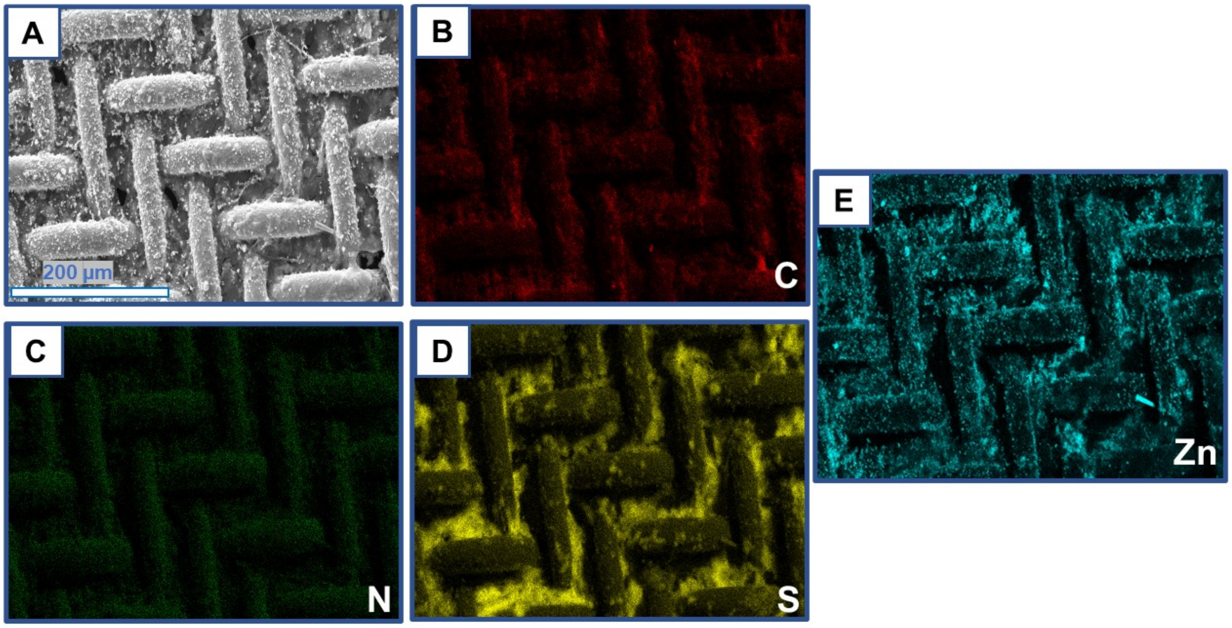

Fig. S24. EDS analysis results of DA-CCP-2 electrode after 1000 cycles. (a) SEM image, (b) EDS map of C, (c) EDS map of N, (d) EDS map of S, (e) EDS map of Zn.

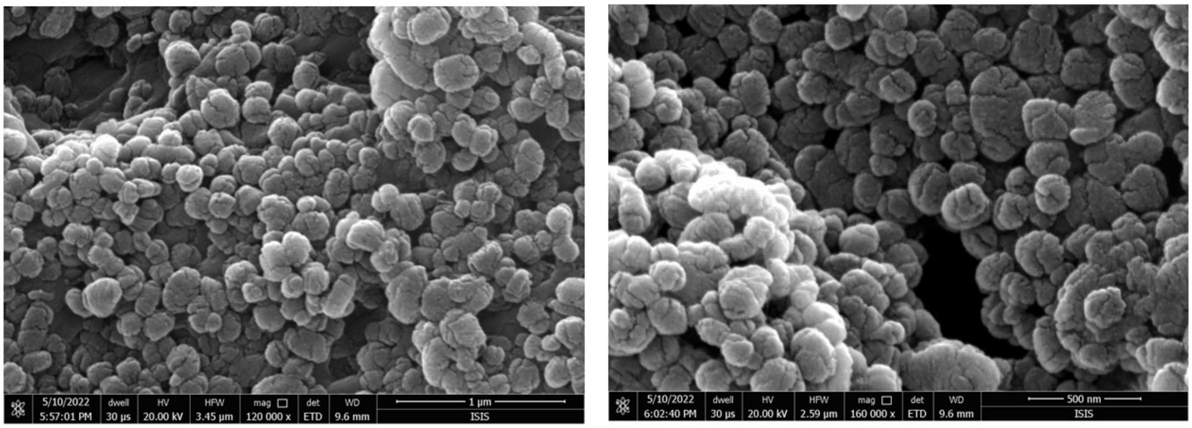

Fig. S25. SEM images of DA-CCP-1 after 1000 cycles.

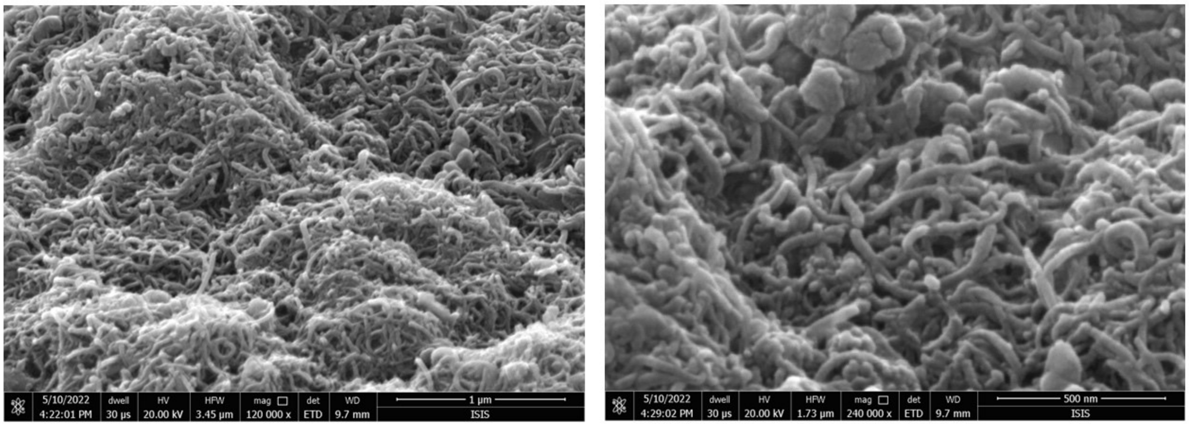

Fig. S26. SEM images of DA-CCP-2 after 1000 cycles.

Section D. Analysis of charge-storage mechanism

1) Ex-situ XPS characterization

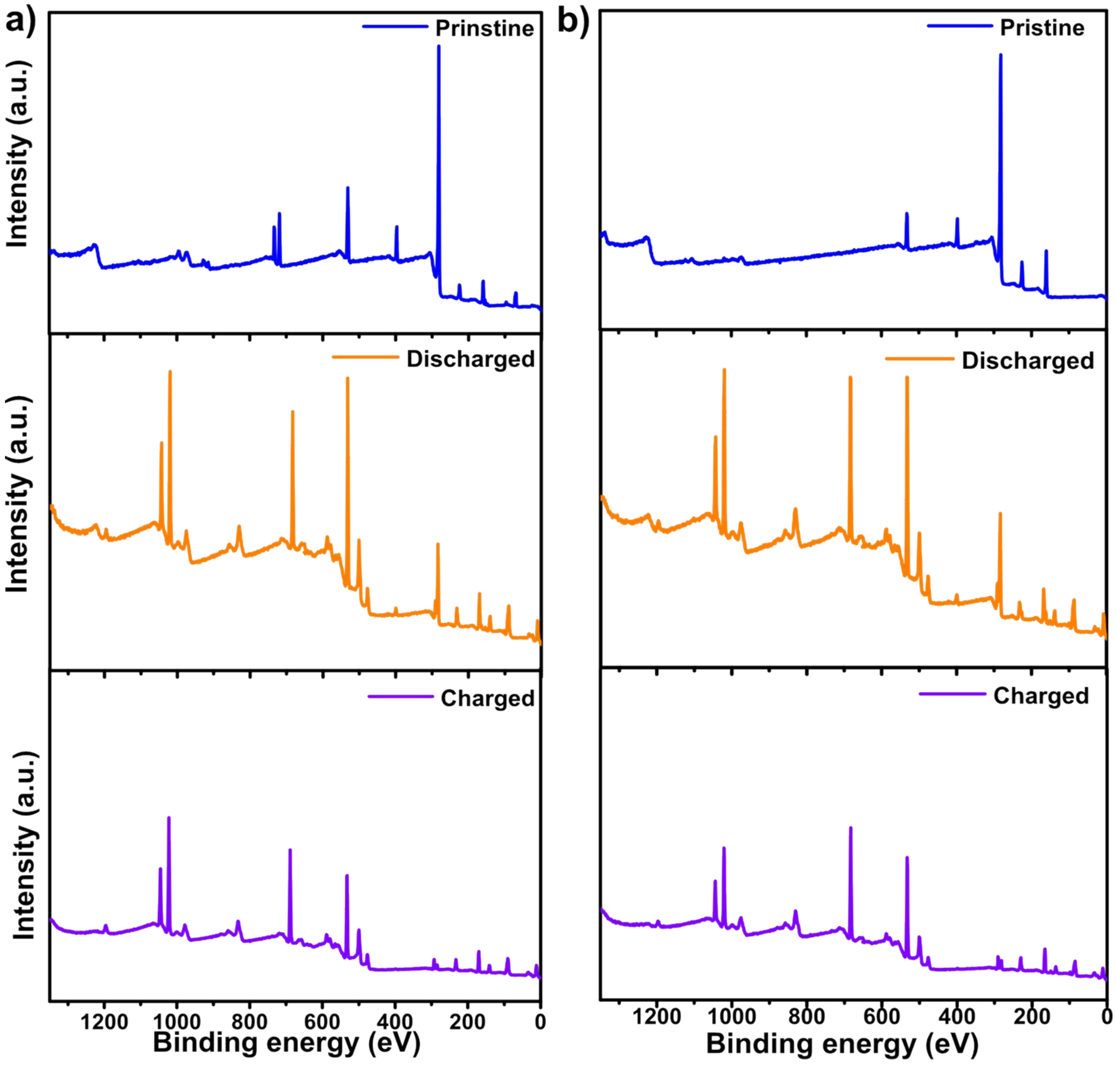

Fig. S27. XPS survey spectra in pristine, charged, and discharged of (a) DA-CCP-1 and (b) DA-CCP-2 cathodes, respectively.

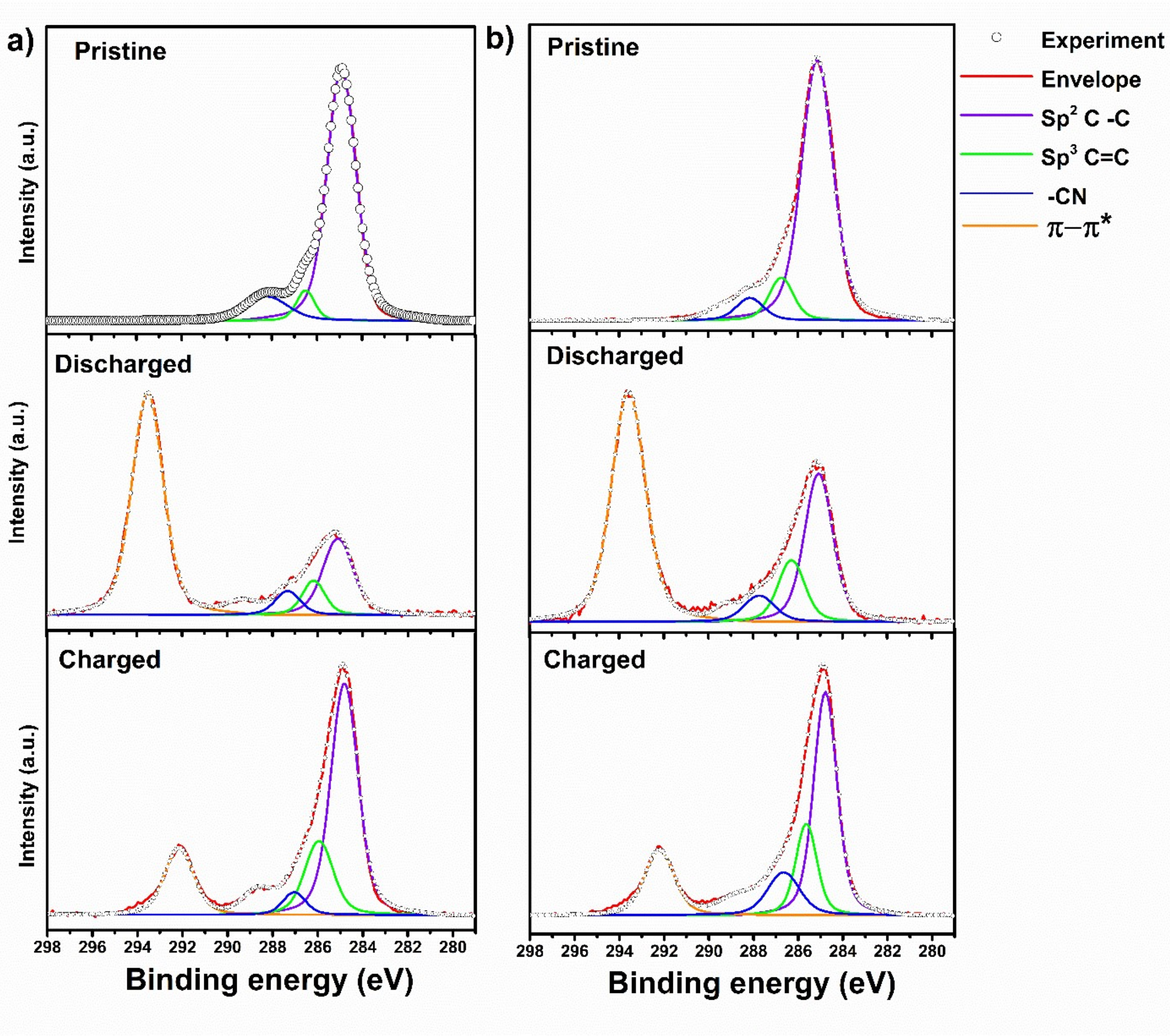

Fig.S28. XPS analysis of C in pristine, charged, and discharged of (a) DA-CCP-1 and (b) DA-CCP-2 cathodes, respectively.

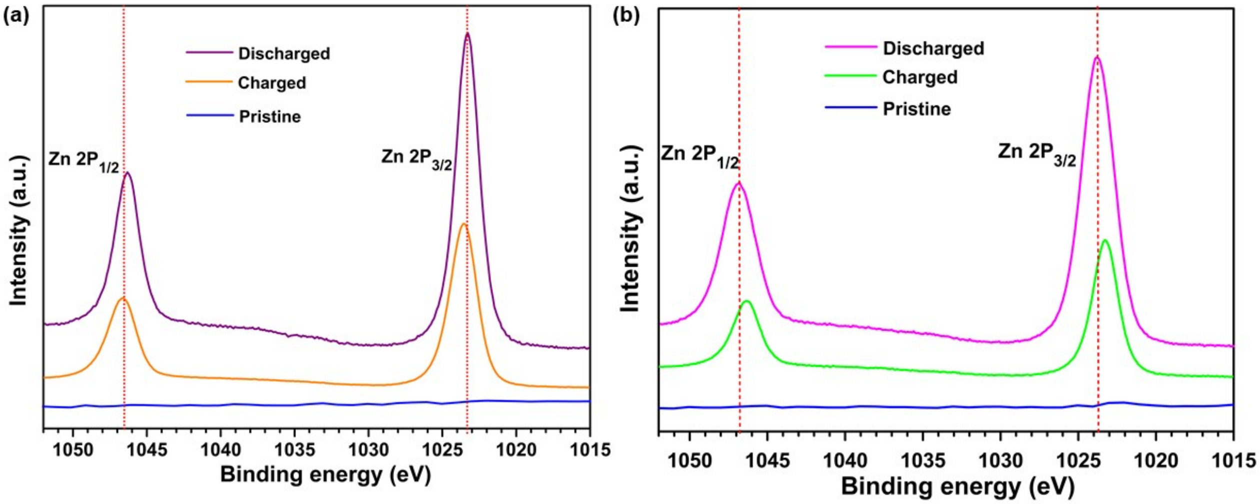

Fig. S29. XPS analysis of Zn^{2+} in pristine, charged, and discharged (a) DA-CCP-1 and (b) DA-CCP-2 cathodes, respectively.

2) Ex-situ FTIR characterization

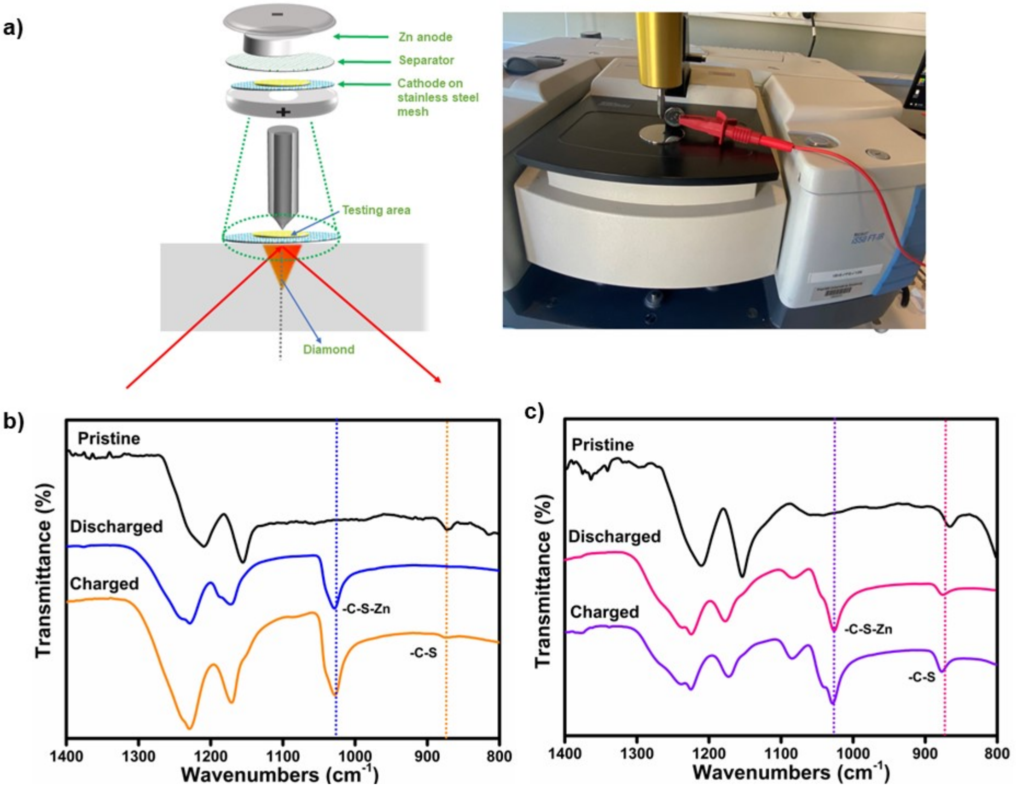

Fig. S30. FTIR characterization of DA-CCP-1 and -2 cathodes in pristine, charged, and discharged states. a) Schematic diagram of ATR-FTIR analysis and optical image of the ATR-FTIR battery device. b) DA-CCP-1 electrode. c) DA-CCP-2 electrode.

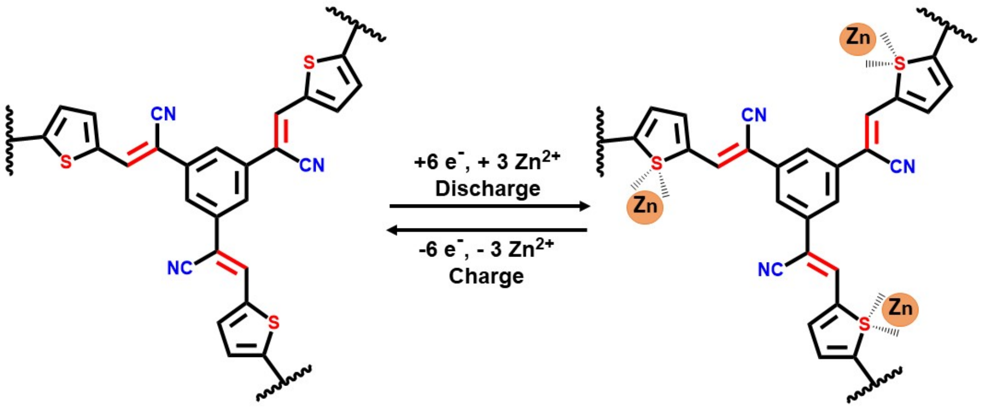

Fig. S31. Proposed 6 e$^-$ (3 Zn^{2+}) reversible electrochemical redox mechanism of DA-CCP cathodes during discharge/charge process.

References:

1. A. Yassin, M. Trunk, F. Czerny, P. Fayon, A. Trewin, J. Schmidt and A. Thomas, *Adv. Funct. Mater.*, 2017, **27**, 1700233.
2. N. Zhang, F. Cheng, Y. Liu, Q. Zhao, K. Lei, C. Chen, X. Liu and J. Chen, *J. Am. Chem. Soc.*, 2016, **138**, 12894-12901.
3. P. He, Y. Quan, X. Xu, M. Yan, W. Yang, Q. An, L. He and L. Mai, *Small*, 2017, **13**, 1702551.
4. J. Guo, J. Ming, Y. Lei, W. Zhang, C. Xia, Y. Cui and H. N. Alshareef, *ACS Energy Lett.*, 2019, **4**, 2776-2781.
5. P. Liu, W. Liu, Y. Huang, P. Li, J. Yan and K. Liu, *Energy Storage Mater.*, 2020, **25**, 858-865.
6. M. Shi, B. Wang, Y. Shen, J. Jiang, W. Zhu, Y. Su, M. Narayanasamy, S. Angaiah, C. Yan and Q. Peng, *Chem. Eng. J.*, 2020, **399**, 125627.
7. Q. Zhao, W. Huang, Z. Luo, L. Liu, Y. Lu, Y. Li, L. Li, J. Hu, H. Ma and J. Chen, *Sci. Adv.*, 2018, **4**, eaao1761.
8. D. Kundu, P. Oberholzer, C. Glaros, A. Bouzid, E. Tervoort, A. Pasquarello and M. Niederberger, *Chem. Mater.*, 2018, **30**, 3874-3881.
9. K. W. Nam, H. Kim, Y. Beldjoudi, T.-w. Kwon, D. J. Kim and J. F. Stoddart, *J. Am. Chem. Soc.*, 2020, **142**, 2541-2548.
10. Y. Wang, C. Wang, Z. Ni, Y. Gu, B. Wang, Z. Guo, Z. Wang, D. Bin, J. Ma and Y. Wang, *Adv. Mater.*, 2020, **32**, 2000338.
11. N. Wang, Z. Guo, Z. Ni, J. Xu, X. Qiu, J. Ma, P. Wei and Y. Wang, *Angew. Chem. Int. Ed*, 2021, **60**, 20826-20832.
12. M. Yu, N. Chandrasekhar, R. K. M. Raghupathy, K. H. Ly, H. Zhang, E. Dmitrieva, C. Liang, X. Lu, T. D. Kühne, H. Mirhosseini, I. M. Weidinger and X. Feng, *J. Am. Chem. Soc.*, 2020, **142**, 19570-19578.
13. W. Wang, V. S. Kale, Z. Cao, S. Kandambeth, W. Zhang, J. Ming, P. T. Parvatkar, E. Abou-Hamad, O. Shekhah, L. Cavallo, M. Eddaoudi and H. N. Alshareef, *ACS Energy Lett.*, 2020, **5**, 2256-2264.
14. A. Khayum M, M. Ghosh, V. Vijayakumar, A. Halder, M. Nurhuda, S. Kumar, M. Addicoat, S. Kurungot and R. Banerjee, *Chem. Sci.*, 2019, **10**, 8889-8894.
15. W. Wang, V. S. Kale, Z. Cao, Y. Lei, S. Kandambeth, G. Zou, Y. Zhu, E. Abouhamad, O. Shekhah, L. Cavallo, M. Eddaoudi and H. N. Alshareef, *Adv. Mater.*, 2021, **33**, 2103617.
16. D. Ma, H. Zhao, F. Cao, H. Zhao, J. Li, L. Wang and K. Liu, *Chem. Sci.*, 2022, **13**, 2385-2390.
17. X. Yue, H. Liu and P. Liu, *ChemComm*, 2019, **55**, 1647-1650.
18. C. Zhang, W. Ma, C. Han, L.-W. Luo, A. Daniyar, S. Xiang, X. Wu, X. Ji and J.-X. Jiang, *Energy Environ. Sci*, 2021, **14**, 462-472.